



1 **The statistical emulators of GGCM phase 2: responses of year-to-year**
2 **variation of crop yield to CO₂, temperature, water and nitrogen**
3 **perturbations**

4
5 Weihang Liu^{1,2,3,4}, Tao Ye^{1,2,3,4*}, Christoph Müller⁵, Jonas Jägermeyr^{5,6,7}, James A.
6 Franke^{8,9}, Haynes Stephens^{8,9}, Shuo Chen^{1,2,3,4}

7
8 ¹ State Key Laboratory of Earth Surface Processes and Resource Ecology (ESPRE),
9 Beijing Normal University, Beijing, 100875, China

10 ² Key Laboratory of Environmental Change and Natural Disasters, Ministry of
11 Education, Beijing Normal University, Beijing 100875, China

12 ³ Academy of Disaster Reduction and Emergency Management, Ministry of
13 Emergency Management and Ministry of Education, Beijing 100875, China

14 ⁴ Faculty of Geographical Science, Beijing Normal University, Beijing 100875, China
15 ⁵ Potsdam Institute for Climate Impact Research (PIK), Member of the Leibniz
16 Association, Potsdam, Germany

17 ⁶ NASA Goddard Institute for Space Studies, New York City, New York, USA

18 ⁷ Center for Climate Systems Research, Columbia University, New York City, New
19 York, USA

20 ⁸ Department of the Geophysical Sciences, University of Chicago, Chicago, Illinois,
21 USA

22 ⁹ Center for Robust Decision- making on Climate and Energy Policy (RDCEP),
23 University of Chicago, Chicago, Illinois, USA

24

25

26 *** Corresponding author at:**

27 State Key Laboratory of Earth Surface Processes and Resource Ecology (ESPRE),

28 Beijing Normal University, 19 Xijiekouwai Street, Beijing, 100875, China.

29 E-mail: yetao@bnu.edu.cn

30



31 **Abstract**

32 Understanding the impact of climate change on year-to-year variation of crop yield is
33 critical to global food stability and security. While crop model emulators are believed
34 to be lightweight tools to replace the models per se, few emulators have been
35 developed to capture such interannual variation of crop yield in response to climate
36 variability. In this study, we developed a statistical emulator with machine learning
37 algorithm to reproduce the response of year-to-year variation of four crop yield to CO₂
38 (C), temperature (T), water (W) and nitrogen (N) perturbations defined in the Global
39 Gridded Crop Model Intercomparison Project (GGCMI) phase 2 experiment. The
40 emulators were able to explain more than 92% variance of simulated yield and
41 performed well in capturing the year-to-year variation of global average and gridded
42 crop yield over current croplands in the baseline. With the changes in CTWN
43 perturbations, the emulators could well reproduce the year-to-year variation of crop
44 yield over most current cropland. The variation of R and the mean absolute error was
45 small under the single CTWN perturbations and dual factor perturbations. These
46 emulators thus provide statistical response surfaces of yield, including both its mean
47 and interannual variability, to climate factors. They could facilitate spatiotemporal
48 downscaling of crop model simulation, projecting the changes in crop yield variability
49 in the future, and serving as a lightweight tool of multi-model ensemble simulation. The
50 emulators enhanced the flexibility of crop yield estimates and expanded the application
51 of large-ensemble simulation of crop yield under climate change.

52 **1. Introduction**

53 The impact of climate change on crop yield is an increasing concern of global food
54 security (Kinnunen et al., 2020). Two distinct approaches have been used to evaluate
55 the impact of climate change on crop yield, process-based crop models and statistical
56 models. Process-based crop models are reliable tools to project crop yields under future



57 climate change but computationally expensive (Jones et al., 2017). In contrast,
58 statistical models are lightweight tools that could fit yield response to historical climate
59 change (Li et al., 2019b) but the relationship between climate factors and crop yield is
60 limited by the current climate conditions. Therefore, it is promising to develop tools
61 that can reduce the expense of computation and increase capacity for flexible future
62 projections (Franke et al., 2020a).

63

64 Earlier studies have developed statistical emulators of process-based crop model results
65 to balance the advantages and disadvantages of process-based crop models and
66 statistical models. Those statistical emulators were initially developed with “entire
67 scenarios” (simultaneous changes in climate factors) simulation during historical or
68 future periods. Emulators have been developed for process-based crop models, like
69 APSIM (Shahhosseini et al., 2019), GEPIC (Folberth et al., 2019), GWG (Xu et al.,
70 2021), GAZE (Raimondo et al., 2021), and WOFOST (Tartarini et al., 2021), and used
71 to estimate historical crop yield. As the emulator trained by historical simulation could
72 not project the crop yield in the future, multiple crop model ensemble simulation in
73 future climate scenarios were used to calibrate emulators (Blanc, 2017, 2020; Blanc
74 and Sultan, 2015; Mistry et al., 2017; Ostberg et al., 2018). However, The scenario-
75 based future crop yield projection is not a systematic perturbation of climate factors
76 change (Franke et al., 2020a).

77

78 An alternative emulation based on “perturbated factors” training dataset was introduced,
79 which offers advantages to separate effects of crop yield drivers. The perturbated factors
80 emulation was first conducted on site-based crop model simulations, which could
81 estimate the yield across a broad range of CO₂, temperature and water (Fronzek et al.,
82 2018; Makowski et al., 2015; Pirttioja et al., 2015) but these emulators were limited to
83 the site-level. To break the constrain of site-based simulation, the global gridded crop
84 model intercomparison (GGCMI) phase 2 provided a simulation dataset across
85 structured CO₂-Temperature-Water-Nitrogen (CTWN) perturbation cubes. This dataset



86 offered two major advantages: it allows for separating the effects of different climatic
87 factors and of nitrogen levels on crop yields, and to distinguish the climatological-mean
88 and year-to-year variation of yields (Franke et al., 2020b). The phase 2 dataset was
89 published to support the derivation of crop yield- climate change “response surfaces”.
90 Based on the CTWN cubes, a statistical emulator has been developed providing near-
91 global-coverage multi-model emulators of climatological-mean yield projections from
92 the GGCM Phase 2 ensemble by using a regression model with a third-order
93 polynomial basis function (Franke et al., 2020a). Due to the focus on climatological-
94 mean yield, the aspect of year-to-year variation of yield under CTWN perturbations has
95 not been fully analyzed or exploited in emulator design.

96

97 For climate change risk assessment, interannual yield variability (or the year-to-year
98 variation of yield) is an important metric of yield risk (Liu et al., 2021b) and food supply
99 stability (Liu et al., 2021a) but has been insufficiently addressed in previous studies
100 (Campbell et al., 2016). Large year-to-year variation of crop yield can influence
101 livelihoods of producers, food prices (Hasegawa et al., 2021), hunger (Janssens et al.,
102 2020) and even lead to political instabilities (Sternberg, 2011). Recently, year-to-year
103 variation has been introduced as a metric for climate change risk on global crop
104 production (Jägermeyr et al., 2021). Developing statistical emulators that can reproduce
105 the year-to-year variation of yield from the CTWN cubes could therefore provide a
106 powerful tool for studies focusing on the risk of climate change impact on yield. In this
107 study, we aimed exclusively to develop statistical emulators to reproduce year-to-year
108 yield variation with GGCM phase 2 experiment data.

109 **2. Data and Methods**

110 **2.1 Data**

111 The input and output data for the simulation of global gridded crop yield were obtained
112 from the GGCM phase 2 experiment dataset, which includes gridded crop yield



113 projections at 0.5° longitudinal/latitudinal resolution for maize, spring wheat, winter
114 wheat, rice, and soybean (Franke et al., 2020b). The input data for the process-based
115 simulations in GGCM Phase 2 included data of climate, soil, atmospheric CO₂
116 concentration, and nitrogen fertilizer application rates. Baseline (1980-2010) climate
117 inputs were used from the AgMIP Modern-Era Retrospective Analysis for Research and
118 Applications (AgMERRA) forcing dataset, including daily maximum and minimum
119 temperatures, precipitation, and solar radiation (Ruane et al., 2015). Systematic
120 perturbations were conducted in each grid cell with seven temperature levels (from -1
121 K to +6 K in 1K interval, with +5K skipped), nine precipitation levels (from -50% to
122 +30%, in 10% interval, with -40% skipped, the Winf precipitation level is simulation
123 under fully irrigated condition), four CO₂-concentration levels (360, 510, 660, and 810
124 ppm), and three nitrogen levels (10, 60, and 200 kg/ha). Simulations were repeated for
125 two adaptation strategies, i.e. no adaptation in cultivar (A0) and adaptation by
126 maintaining growing season length (A1). Twelve GGCMs were then forced with each
127 of these perturbations of the original reanalysis weather data. We selected 10 of 12 crop
128 models in the GGCM phase 2 experiment for constructing the emulators. These were
129 APSIM-UGOE, CARAIB, EPIC-IIASA, EPIC-TAMU, GEPIC, LPJ-GUESS, LPJmL,
130 ORCHIDEE-crop, pDSSAT, and PEPIC (Table 1). PROMET and JULES were not
131 included as they used different climate inputs.

132

133 The GGCMs used a national and subnational crop calendar for crops that is based on
134 Sacks et al (2010), Portmann et al (2010), and environment-based extrapolations
135 (Elliott et al., 2015). The crop calendar was used to determine the window to calculate
136 the climatic predictors and grid-specific growing season length. The current global
137 harvested area for identifying currently used cropland was obtained from the spatial
138 production allocation model (SPAM) whose spatial resolution was 10km. The soil type
139 data was obtained from the Harmonized World Soil Database (Nachtergaele et al.,
140 2009).

141

142 **Table 1** GGCMs included in emulation. Each model offers the same set of CTWN simulations across



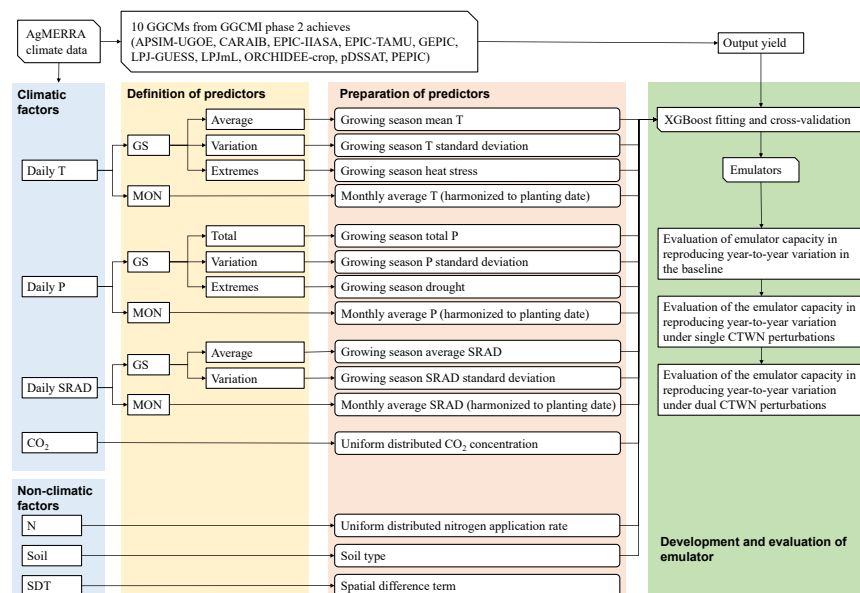
143 four crops.

GGCMs	Maize	Winter wheat	Spring wheat	Rice
APSIM-UGOE	✓	✓	✓	✓
CARAIB	✓	✓	✓	✓
EPIC-IIASA	✓	✓	✓	✓
EPIC-TAMU	✓	✓	✓	✓
GEPIC	✓	✓	✓	✓
LPJ-GUESS	×	✓	✓	×
LPJmL	✓	✓	✓	✓
ORCHIDEE-crop	✓	✓	×	✓
pDSSAT	✓	✓	✓	✓
PEPIC	✓	✓	✓	✓

144 * LPJ-GUESS omits maize and rice, and ORCHIDEE-crop omits spring wheat (denoted by “×”)

145 2.2 Methods

146 Our study focused on the development and evaluation of emulators, which contains the
 147 following steps: 1) defining the predictors used to train the emulators; 2) preparing the
 148 predictors with climatic and non-climatic data; 3) training and cross validating the
 149 emulators with machine learning algorithm; and 4) evaluating the performance of
 150 emulators (Figure 1).



151
 152 **Figure 1** Overall framework of emulator development for GGCMs. Each GGCM-crop combination was
 153 calibrated as an emulator independently. T: temperature, processed separately for daily maximum, and



154 minimum temperatures, P: precipitation, SRAD: solar radiation, N: nitrogen, Soil: soil properties. When
155 developing irrigated yield emulator, the precipitation-related predictors are excluded.

156 **2.2.1 Definition and preparation of predictors**

157 All the predictors were computed or adapted from the GGCMs' input and output
158 datasets. The climatic predictors were defined at two time-scales, growing season (GS)
159 and monthly (MON) (Table 2). The growing season average temperature, total
160 precipitation and average solar radiation were able to explain the variation of
161 climatological mean yield of GGCM phase2 (Franke et al., 2020a). To improve the
162 capacity of emulators in reproducing the year-to-year variation of crop model yield,
163 daily variability and extremes of climate factors during the growing seasons were
164 considered here. The variation of temperature, precipitation and solar radiation during
165 the growing seasons were calculated with the standard deviation of their daily values in
166 each growing season, which represents the intensity of daily fluctuation of weather.
167 Additionally, the heat and drought were selected to be the extreme climate predictors,
168 which was quantified by extreme degree day (EDD, cumulative temperature that exceed
169 the high temperature threshold, Lobell et al., 2012) and maximum consecutive drought
170 day (CDD, maximum length of consecutive days without precipitation, Troy et al.,
171 2015), because the negative effect of these two extremes could be shown by the current
172 GGCM (Heinicke et al., 2022). Other climate extremes, like excessive wetness, was not
173 used because the GGCM failed to show the negative effect (Li et al., 2019a; Liu et al.,
174 2022).

175
176 The monthly predictors only consisted of monthly average values. The monthly average
177 temperature, total precipitation and average solar radiation were harmonized according
178 to the specific planting date. The number of months was determined with the crop-
179 specific maximum growing season length over the global cropland defined by GGCM
180 phase2 experiment. For winter and spring wheat, we prepared the climatic predictors
181 over 10 and eight months after sowing. For maize and rice, climatic predictors over
182 eight and seven months after sowing were used, respectively.



183

184 The atmospheric CO₂ concentration and the nitrogen application rate were uniformly
185 distributed predictors. All years and grid cells were set at the same CO₂ concentration
186 and nitrogen application rate for each perturbation. Soil property is an important
187 temporally constant predictor, whose interaction with climate played important role in
188 yield simulation and emulator development (Blanc, 2017). As the soil parameter
189 settings of each GGCM varied, we selected the soil type at each grid to represent the
190 spatial variation of soil properties. There were 13 soil types, including heavy clay, silty
191 clay, light clay, silt clay loam, clay loam, silt, silt loam, sandy clay, loam, sandy clay
192 loam, sandy loam, loamy sand, sand. The most obvious difference across cultivars over
193 the global croplands is the growing degree requirement to reach maturity, which was
194 determined by both mean climatology and cultivar traits. To reproduce the spatial
195 difference of simulated crop yield, we added a spatial difference term as a predictor, i.e.
196 temporal constant growing season length.

197

198 As the purpose of emulator training is to develop a lightweight tool for crop simulation,
199 there has always been a trade-off between the goodness-of-fit and the number of
200 predictors. Therefore, we considered three strategies of using our predictors. “Strategy
201 A” uses all predictors (the “Full” model), which is expected to derive the best goodness-
202 of-fit. “Strategy B” uses only climatic predictors during growing season scale (the “GS”
203 model), together with CO₂ concentration, nitrogen application rate and site information,
204 soil class and growing season length. “Strategy C” uses only monthly average climatic
205 predictors with other location-invariant predictors (the “Mon” model). In general,
206 strategy B uses the smallest number of predictors, but those predictors need to be
207 computed from daily climate forcing. Stagey C only relays on monthly climate data,
208 and therefore is the least costly strategy for data preparation. A comparison between the
209 three strategies would help us find a good balance between the predictors used and
210 overall goodness-of-fit of the emulators.

211

212 **Table 2** Predictors of emulation. For rainfed yield emulators, we used all these predictors but for fully-



213 irrigated yield emulators, the precipitation predictors were not included. Full, GS and Mon were three
 214 strategies to develop emulators. Full: developing emulators with all the climatic predictors; GS:
 215 developing emulators with climatic predictors during growing season scale; Mon: developing emulators
 216 with climatic predictors during monthly scale.

Predictor abbreviations	Descriptions	References	Full	GS	Mon
Temperature related predictors					
GDD _{low-high_GS}	Growing degree day during growing season (winter wheat: low=0°C, high=30°C; spring wheat: low=5°C, high=30°C; maize: low=8°C, high=30°C; rice: low=10°C, high=35°C)	(Frieler et al., 2017; Jägermeyr et al., 2020; Lobell et al., 2012)			
EDD _{high+_GS}	Extreme degree day during growing (winter and spring wheat, maize: high=30°C; rice: high=35°C)	(Lobell et al., 2012)			
Tmax_GSmean	Average daily maximum temperature during growing season	(Zhu and Troy, 2018)			
Tmin_GSmean	Average daily minimum temperature during growing season	(Zhu and Troy, 2018)			
Tmax_GSstd	Standard deviation of daily maximum temperature during growing season	(Zhu and Troy, 2018)			
Tmin_GSstd	Standard deviation of daily minimum temperature during growing season	(Zhu and Troy, 2018)			
Tmax_MONmean	Harmonized monthly average daily maximum temperature (MON=1–10 for winter wheat, MON=1–8 for spring wheat and maize, MON=1–7 for rice, since planting date)	(Folberth et al., 2019) (Jägermeyr et al., 2020)			
Tmin_MONmean	Harmonized monthly average daily minimum temperature (MON=1–10 for winter wheat, MON=1–8 for spring wheat and maize, MON=1–7 for rice, since planting date)	(Folberth et al., 2019) (Jägermeyr et al., 2020)			
Precipitation related predictors					
Pre_GSsum	Total daily precipitation during growing season	(Troy et al., 2015)			
Pre_GSstd	Standard deviation of daily precipitation during growing season	(Zhu and Troy, 2018)			
CDD_GS	Consecutive drought day (daily precipitation=0)	(Troy et al., 2015)			
Pre_MONsum	Harmonized monthly total precipitation (MON=1–10 for winter wheat,	(Folberth et al., 2019)			



	MON=1–8 for spring wheat and maize, (Jägermeyr et al., MON=1–7 for rice, since planting date) 2020)			
Solar radiation related predictors				
SRAD_GSmean	Average daily solar radiation during growing season	(Folberth et al., 2019)		
SRAD_GSstd	Standard daily solar radiation during growing season	(Folberth et al., 2019)		
SRAD_MONmean	Harmonized monthly average daily solar radiation (MON=1–10 for winter wheat, MON=1–8 for spring wheat and maize, MON=1–7 for rice, since planting date)	(Folberth et al., 2019) (Jägermeyr et al., 2020)		
Greenhouse gas concentration				
CO ₂	CO ₂ concentration	(Franke et al., 2020a)		
Non-climatic predictors				
N	Nitrogen fertilizer application	(Franke et al., 2020a)		
Soil_type	Soil type	(Blanc, 2017)		
SDT	Spatial difference term	(Folberth et al., 2019)		

217 *The colored the row denotes the predictors was included in the emulator.

218 2.2.2 Emulator training and validation

219 Training the emulator of specific GGCM is to derive the response relationship between
 220 input and output, so that the emulator could replicate the complex process of yield
 221 simulation within the crop model. Emulation was trained by using machine learning
 222 regression on the GGCM-2 ensemble of crop- specific simulated yield with all CTWN
 223 perturbations. Each grid-year-perturbation combination was regarded as a sample in the
 224 fitting. We developed emulators of irrigated and rainfed yield and in A0 and A1
 225 scenarios separately. Since the outputs of GGCM outside the current croplands were
 226 not well examined, we trained the machine learning based emulators only on currently
 227 used cropland, according to the SPAM data for each crop separately.

228

229 The extreme gradient boosting (XGBoost) algorithm, a highly efficient realization of
 230 the gradient boosting approach that showed the best performance in recent machine
 231 learning challenges (Chen and Guestrin, 2016), was used to train the emulators. Key



232 parameters in XGBoost, including the learning rate (0.1), the number of estimators
233 (4000), and the maximum tree depths (10), were tuned by a grid search along parameter
234 dimensions based on the default parameter as reference (Folberth et al., 2019). The
235 goodness-of-fit of XGBoost was validated with the coefficient of determination R^2_{adjust} .

$$236 \quad R^2_{\text{adjust}} = 1 - \frac{(n-1) \times (1-R^2)}{n-k}$$

237 where n is the sample size of the validation set, k is the number of predictors.

238

239 We used two validation strategies to show the goodness-of-fit. Firstly, we used a 10-
240 fold cross-validation that the samples were randomly divided into 10 folds, with nine
241 of them used for training, and the rest used for validation. Secondly, considering the
242 spatial autocorrelation in the raw GGCM simulated yield can invalidate the machine
243 learning random selected validation sets (Ploton et al., 2020), we used the Köppen-
244 Geiger climate regions to split the trained and validated sets. We used a leave-one-out
245 approach that 29 out of the 30 climate regions were used for training, and the rest used
246 for validation. The climate regions which contain less than 50 grids under current
247 harvested areas will be removed from leave-one-out cross validation process.
248 Emulators were trained in Python3.8 with GPU
249 (<https://xgboost.readthedocs.io/en/latest/python/index.html>).

250 2.2.3 Evaluation of emulator

251 Emulator performance was evaluated by comparing the 30-year emulated yield with the
252 30-year simulated yield of the GGCM. As we aimed at developing emulator that could
253 replicate the year-to-year variation of yield, the correlation coefficient (R), mean
254 absolute error (MAE) and mean relative error (MRE) were used to evaluate the
255 performance of emulators in the baseline and varied perturbations.

$$256 \quad R = \frac{\sum_{i=1}^n (Y_{XGB,i} - \bar{Y}_{XGB})(Y_{GGCM,i} - \bar{Y}_{GGCM})}{\sqrt{\sum_{i=1}^n (Y_{XGB,i} - \bar{Y}_{XGB})^2 \cdot (Y_{GGCM,i} - \bar{Y}_{GGCM})^2}}$$



257
$$MAE = \frac{\sum_{i=1}^n |Y_{XGB,i} - Y_{GGCM,i}|}{n}$$

258
$$MRE = \frac{\sum_{i=1}^n |(Y_{XGB,i} - Y_{GGCM,i}) / Y_{GGCM,i}|}{n}$$

259 where n is the sample size of the validation set, $Y_{GGCM,i}$ is the annual simulated yield
260 of the GGCMs, $Y_{XGB,i}$ is the annual projected yield of the XGB algorithm, and \bar{Y}_{XGB}
261 and \bar{Y}_{GGCM} were the average XGBoost predicted and GGCM simulated yield,
262 respectively.

263 3. Results

264 3.1 Goodness-of-fit of the emulators training

265 Overall, the emulator developed with XGBoost algorithm could well reproduce the
266 variance of GGCM yield simulations, with adjusted R^2 greater than 0.92 (Table 3). The
267 scatter plots of emulated yield and GGCM simulated yield for testing samples are
268 clustered closely around the 1:1 ratio line (Figure S1). For most emulators the adjusted
269 R^2 under fully-irrigated (Winf) simulation were greater than those under rainfed
270 simulation (W). Under A0 and A1 scenarios, the adjusted R^2 was comparable. For
271 different crops, the performance of emulators developed for winter and spring wheat
272 were slightly better than those developed for maize and rice. Among the GGCMs,
273 EPIC-IIASA's behavior can best be emulated by emulators, with greatest R^2 values for
274 all crops and scenarios. There are also several GGCM that is bit challenging for the
275 XGB algorithm to capture, i.e. winter wheat and spring wheat simulation from GEPIC,
276 maize of pDSSAT, and rice of EPIC-TAMU, with R^2 values ranging from 0.92 to 0.96.
277 When using the Köppen–Geiger climate regions to apply the leave-one-out cross
278 validation, the adjusted R^2 is generally smaller than those obtained by the 10-fold cross
279 validation with randomly selected samples, ranging between 0.93 and 0.64 (Table S1).

280
281 **Table 3** Adjusted R^2 of XGBoost derived from 10-fold cross validation with randomly selected samples



GGCMs (A0)	Winter wheat		Spring wheat		Maize		Rice	
	Winf	W	Winf	W	Winf	W	Winf	W
APSIM-UGOE	0.99	0.97	0.98	0.97	0.92	0.94	0.96	0.96
CARAIB	0.98	0.98	0.98	0.98	0.97	0.97	0.98	0.97
EPIC-IIASA	0.99	0.98	0.99	0.99	0.99	0.98	0.99	0.98
EPIC-TAMU	0.97	0.97	0.97	0.97	0.94	0.97	0.93	0.97
GEPIC	0.97	0.95	0.98	0.96	0.97	0.95	0.97	0.96
LPJ-GUESS	0.99	0.98	0.99	0.98	-	-	-	-
LPJmL	0.98	0.98	0.98	0.98	0.94	0.96	0.95	0.96
ORCHIDEE-crop	0.99	0.98	-	-	0.98	0.96	0.97	0.97
pDSSAT	0.97	0.97	0.99	0.98	0.92	0.92	0.95	0.96
PEPIC	0.98	0.97	0.98	0.98	0.98	0.97	0.97	0.97

GGCMs (A1)	Winter wheat		Spring wheat		Maize		Rice	
	Winf	W	Winf	W	Winf	W	Winf	W
APSIM-UGOE	0.99	0.96	0.98	0.96	0.96	0.92	0.97	0.96
CARAIB	0.98	0.98	0.99	0.99	0.97	0.97	0.98	0.97
EPIC-IIASA	-	-	-	-	-	-	-	-
EPIC-TAMU	0.98	0.98	0.97	0.97	0.95	0.97	0.94	0.97
GEPIC	0.98	0.96	0.98	0.97	0.98	0.97	0.98	0.97
LPJ-GUESS	0.99	0.99	0.99	0.99	-	-	-	-
LPJmL	0.98	0.99	0.97	0.98	0.94	0.96	0.97	0.96
ORCHIDEE-crop	-	-	-	-	-	-	-	-
pDSSAT	0.97	0.97	0.98	0.98	0.93	0.92	0.96	0.96
PEPIC	0.98	0.97	0.99	0.98	0.98	0.97	0.97	0.97

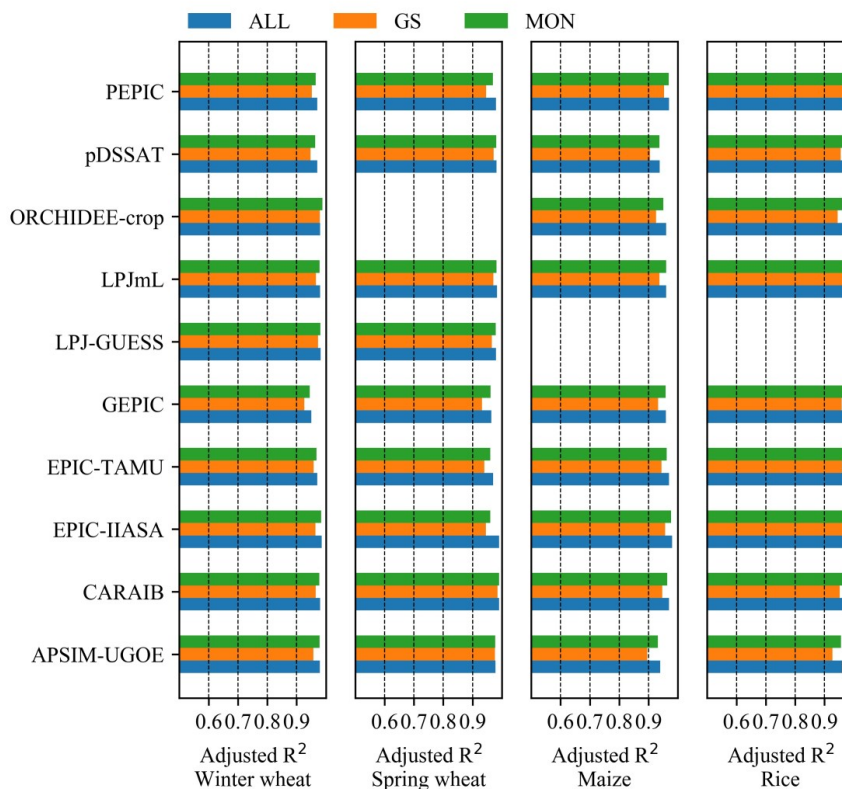
282 “-”: No GGCM simulation; Winf: irrigated condition; W: rainfed condition.

283
 284

285 The adjusted R^2 of emulators developed with all predictors (“Full model”) was greater
 286 than those developed with growing season predictors (“GS model”) and monthly
 287 predictors (“MON model”) (Figure 2). If we validated using the 10-fold randomly
 288 selected sample approach, the performances of “GS model” and “MON model” were
 289 good and comparable to the “Full Model”. Nevertheless, the difference in performance
 290 became much pronounced when validated by using the climate-zone based leave-one-
 291 out approach (Figure S2). GS models would suffer from reduced number of predictors
 292 and their adjusted R^2 s were 0.1~0.15 smaller than corresponding MON models. Still,
 293 Full models had the largest adjusted R^2 at the cost of the largest number of predictors.
 294 For later usage of the emulators, a trade-off must be taken between cost of preparing



295 predictors and model goodness-of-fit, and the “MON model” could be a balanced
 296 choice as it required only monthly average weather conditions.



297
 298 **Figure 2** Adjusted R² of emulators (10-fold cross validation with randomly selected samples) with
 299 different strategy of predictors. All: “Full model”, GS: “GS model”, Mon: “MON model”. Emulators
 300 for ORCHIDEE by spring wheat, and LPJ-GUESS by Maize and Rice were not fitted due to the lack of
 301 simulation of raw GGCM.

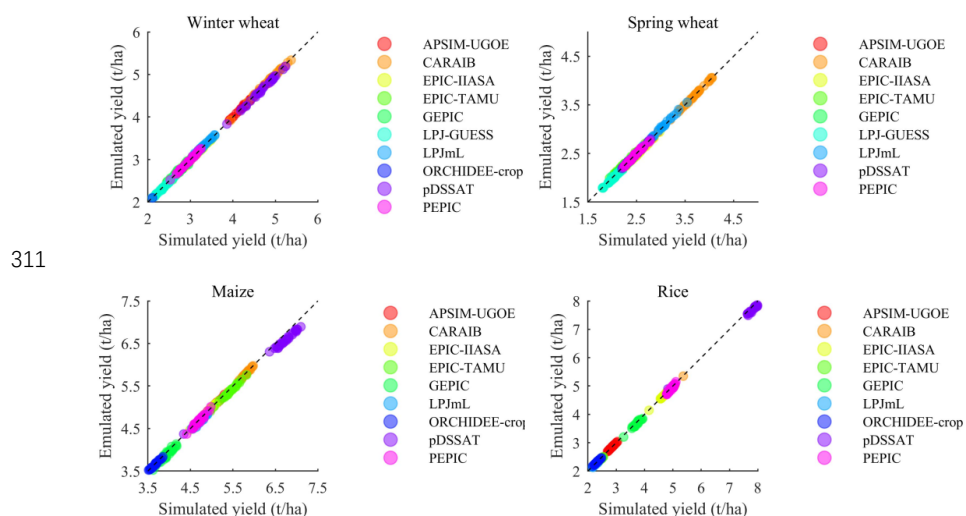
302 3.2 Performance of emulators to capture the year-to-year variation of GGCM 303 yield in the baseline

304 3.2.1 Performance of individual emulators at the global scale

305 Over current global cropland, the emulator of each GGCM could well reproduce the
 306 year-to-year variation of global average yield in the baseline period (during 1981–2010)
 307 (Figure 3). All individual emulators could capture the corresponding GGCM simulated



308 yield, with scatters concentrated in the 1:1 ratio line. Different GGCM simulated yield
309 levels varied from 1.7 to 7.8 t/ha but the performance of emulators has not been
310 influenced.



311

312

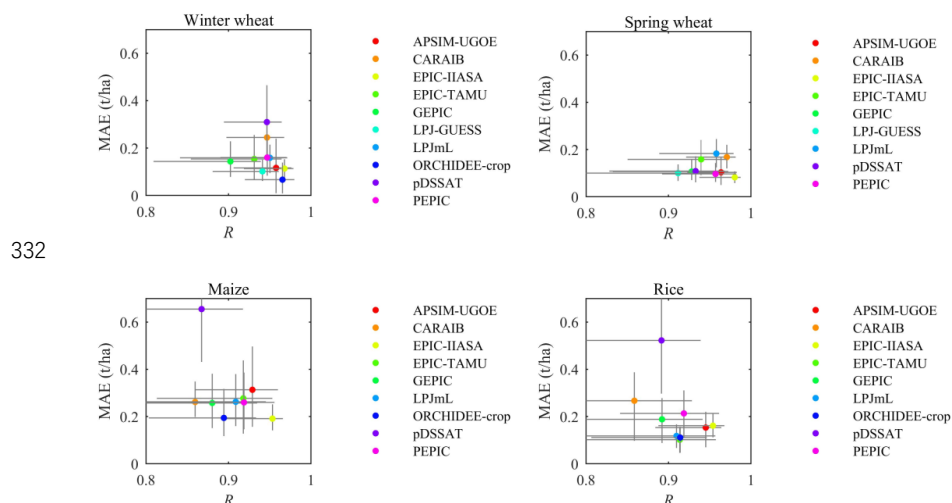
313 **Figure 3** Emulator performance to reproduce the year-to-year variation of global average yield (1981 –
314 2010) over current cropland. As ORCHIDEE-crop has not simulated yield under C360T0W0N200, we
315 used the C360T0W10N200 as the baseline. Each point with the same color is yield in 30 year.

316 3.2.2 Performance of individual emulators at grid scale

317 The overall performances of emulators at grid level were good for most crop-GGCM
318 combinations in the baseline. The performance of each emulator over current global
319 cropland grids were plotted by using scatter of MAE and R (Figure 4). The capacity of
320 emulators in reproducing the wheat yield simulated by GGCMs was better than that of
321 maize and rice. The median R over current winter and spring wheat harvested areas
322 were greater than 0.9. The R of the EPIC-TAMU-emulator and the LPJ-GUESS-
323 emulator were relatively smaller than other eight emulators developed for winter and
324 spring wheat, respectively. The median MAEs over current winter and spring wheat
325 harvested areas were less than 0.4 t/ha and 0.3 t/ha for winter and spring wheat
326 emulators, respectively, and the MAEs of the pDSSAT-emulator and LPJmL-emulator
327 were relatively greater. Over current maize harvested areas, the median R was greater
328 than 0.85 and the median of MAE was less than 0.4 t/ha, except pDSSAT-emulator. The



329 median R of emulators developed for rice were greater than 0.89, and the median MAE
330 were less than 0.3 t/ha over current rice harvested areas, whereas the performances of
331 pDSSAT-emulator and CARAIB-emulator were relatively worse.



332
333
334 **Figure 4** Correlation coefficient (R) and mean absolute error (MAE) over current cropland in the baseline
335 (C360T0W0N200). As the ORCHIDEE-crop has not simulated yield under C360T0W0N200
336 perturbation, we used the C360T0W10N200 as the baseline. The dot denotes the median and the error
337 bar denotes the interquartile range from all grid cells in which the crop is grown according to the
338 SPAM2010 data.

339 3.2.3 Performance of multiple emulators ensemble at grid scale

340 The multi-emulators ensemble median was able to reproduce the year-to-year variation
341 of gridded yield over current cropland in the baseline (C360T0W0N200) from 1981 to
342 2010. The temporal correlation coefficient R between GCM simulated and emulated
343 yield time series over most current harvested areas were greater than 0.8 (multi-model
344 ensemble median) (Figure 5), and the uncertainty (standard deviation) of R across
345 emulators was smaller than 0.2 (Figure S3). The mean absolute error (MAE) and mean
346 relative error (MRE) over most current harvested areas were mostly smaller than 1 t/a
347 and 10%, respectively (Figure S4). The spatial pattern of MRE for four crops all showed
348 a hotspot of large MRE in the Middle East, and for maize the hotspot of great MRE was
349 also found in the southern China (Figure S4).

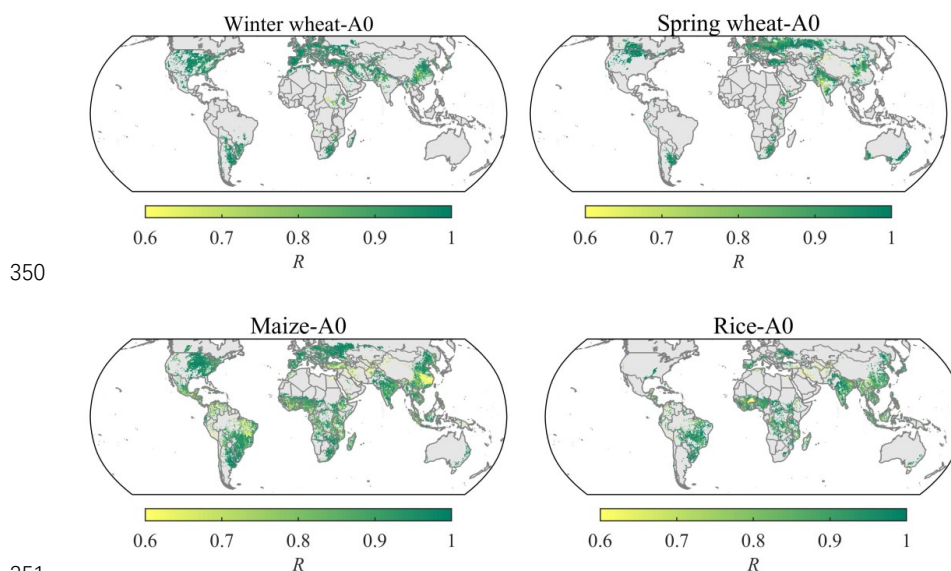


Figure 5 Multi-model ensemble median R in the baseline over current cropland. R : correlation coefficient between simulated and emulated yield time series of each GGCM from 1981 to 2010.

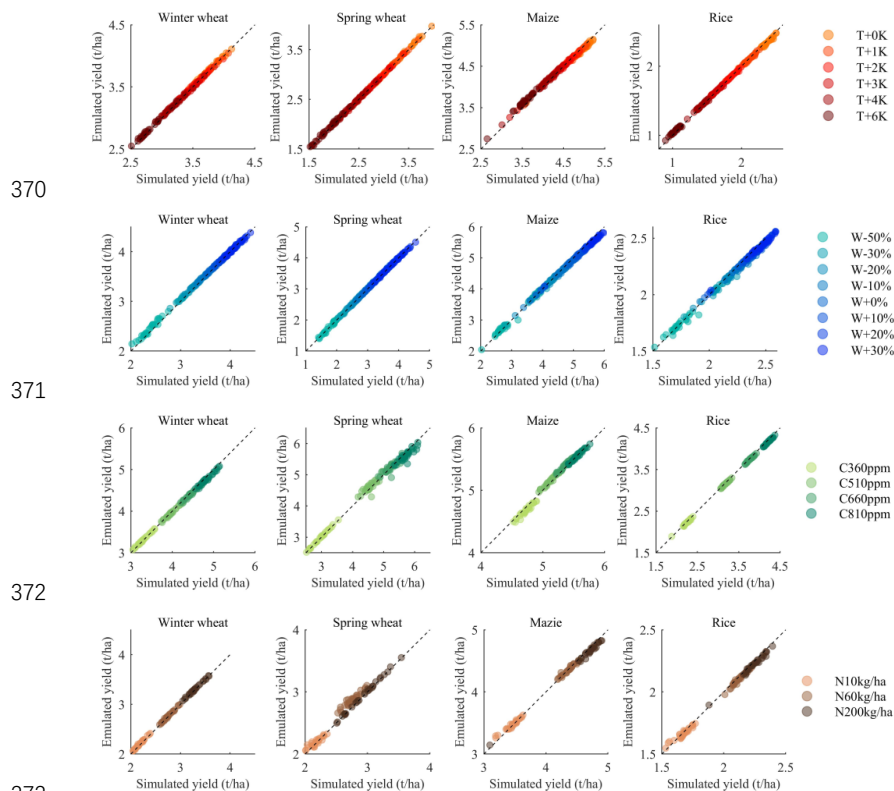
3.3 Performance of emulators to capture the year-to-year variation of GGCM yield in the CTWN cube

3.3.1 Performance of individual emulators at the global scale

357 The agreement of year-to-year variation of global average yield between simulation and
358 emulation was consistent with changes in CTWN cube over present cropland (**Figure 6**).
359 Under varied CTWN perturbations, the emulator could well reproduce the year-to-year
360 variation of global mean yield from 1981 to 2010. Even when the temperature
361 perturbation reached +6K, the emulator was still able to capture the year-to-year
362 variation of global mean yield. Similarly, when the precipitation was less than baseline
363 by 50%, the year-to-year variation of emulated global mean yield was well matched
364 with those of GGCM simulation. Additionally, the fertilizations of elevated CO₂
365 concentration and nitrogen application have been well reproduced by emulator. Similar
366 capacity in reproducing the annual global mean yield was also been found in other
367 emulators (Figure S5). Even under the concurrent warm and drought condition, i.e.



368 T+6K and W-50%, the year-to-year variation of global mean yield could be well
369 reproduced by emulator (Figure S6).



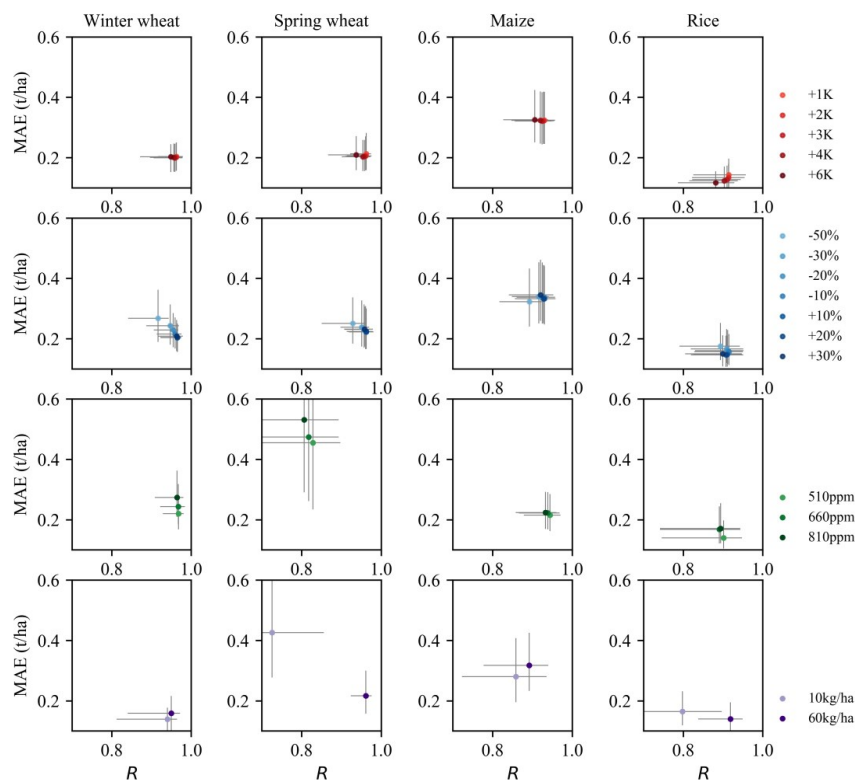
373
374 **Figure 6** Performance of one exemplary emulator (LPJmL-A0) in reproducing the year to year variation
375 of global mean yield from 1981 to 2010 under varied individual CTWN perturbations. Each point with
376 the same color is yield in one year. The performances of other emulators are similar to LPJmL-A0, which
377 can be referred in the Figure S5 for EPIC-TAMU.

378 3.3.2 Performance of individual emulators at the grid scale under single 379 perturbation

380 To illustrate the performance of individual emulators to reproduce annual yield
381 variation, we selected the LPJmL-A0 emulator as an example. The *R*-MAE scatter plots
382 of LPJmL-A0 illustrated the response of gridded accuracy to varied perturbations of
383 CTWN (**Figure 7**). The changes in accuracy of emulators under single CTWN
384 perturbations were small with largest differences in spring wheat for modifications in



385 the CO₂ (C) and nitrogen (N) dimensions, and for rice for modifications in the water
386 (W) dimension. The overall accuracy could be kept on the high level, with greater *R*
387 and smaller MAE. Under temperature perturbations, the median *R*s of emulators for
388 four crops were greater than 0.9, and the range of *R*s was smaller than 0.03. The median
389 MAEs of emulators for four crops were less than 0.35, and the variation of median
390 MAEs was smaller than 0.02 from +1 to +6K perturbations. For precipitation
391 perturbations, the median *R*s of emulators for four crops were greater than 0.88,
392 meanwhile the difference of median *R*s across varied precipitation perturbations was
393 smaller than 0.06. The median MAEs of emulators for four crops was smaller than 0.38,
394 and the range of median MAEs variation was as small as 0.05. The median *R*s and
395 MAEs of emulators for four crops under CO₂ concentration perturbations and nitrogen
396 perturbations were comparable to those under temperature and precipitation
397 perturbations, except for spring wheat. Although the performance of spring wheat
398 emulator under CO₂ and nitrogen perturbations was not as good as other crops, the
399 median *R*s was still greater than 0.75 and the median MAEs were smaller than 0.2.
400 Similar pattern of other emulators' performances under single perturbations at grid scale
401 are shown in the Table S2 and Table S3.



402
403 **Figure 7** R -MAE scatter of the exemplary emulator (LPJmL-A0) under varied single CTWN
404 perturbations. Each dot denotes the median of R or MAE over current cropland, the error bar denotes the
405 interquartile range. R : correlation coefficient, MAE: mean absolute error. More details of other emulators
406 can refer to Table S2 and S3.

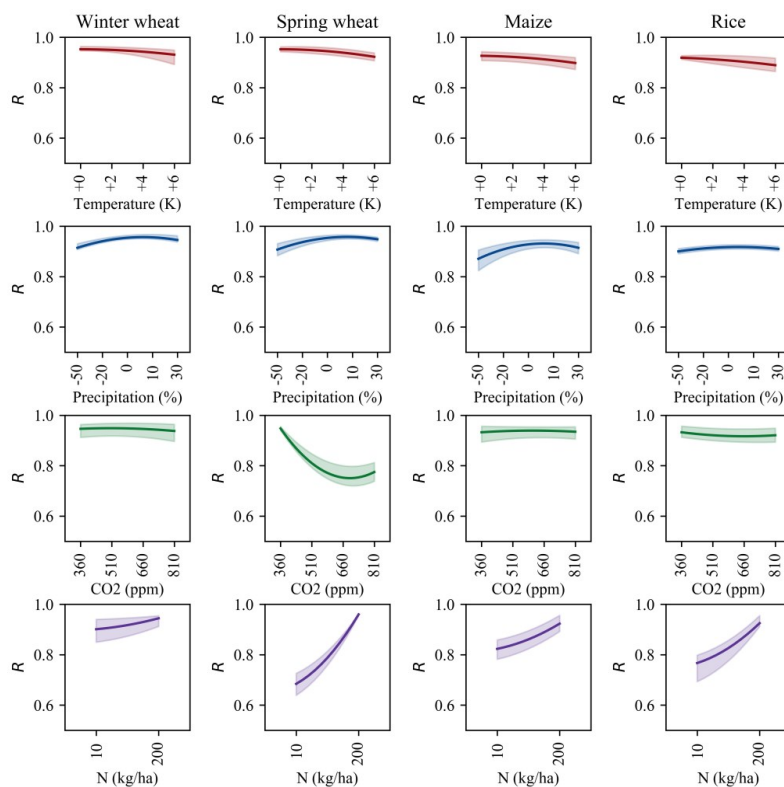
407 3.3.3 Performance of multiple emulators ensemble at the grid scale under single 408 perturbation

409 When looking at the ensemble of multiple emulators, the R s and MAEs under CTWN
410 cubes was not divergent obviously (Figure 8, Figure 9).

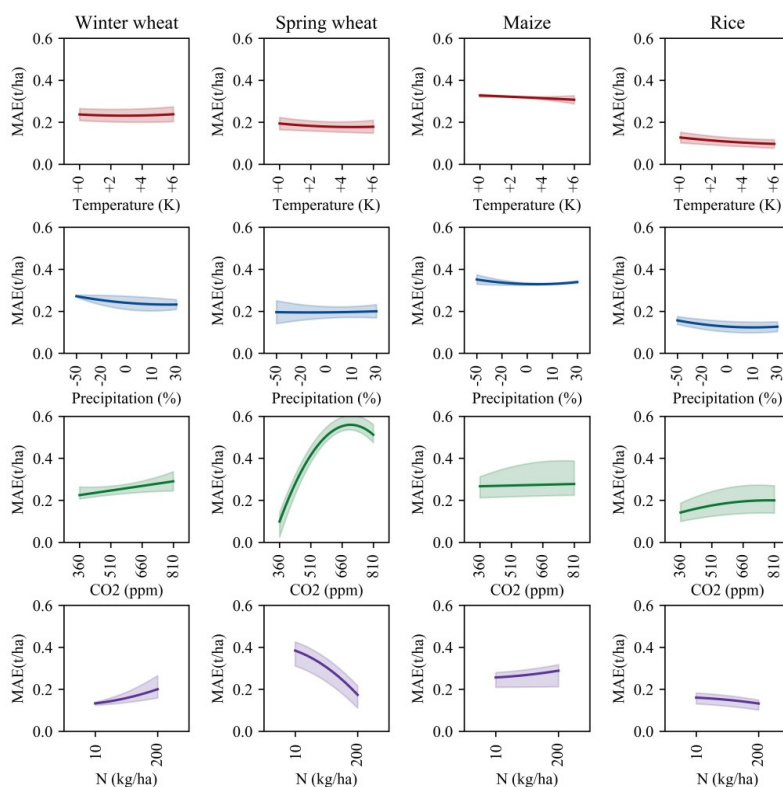
411
412 Under temperature perturbations, the range of model-ensemble median R s across
413 multiple emulators was smaller than 0.01, and the range of median MAEs was as small
414 as 0.03t/ha. For precipitation perturbation, the difference in median R s was less than
415 0.03, and the changes in median MAEs was less than 0.09t/ha. Under the perturbation



416 of CO₂ concentration, the emulators for winter wheat, maize and rice showed a greater
 417 median R s which ranged from 0.96 to 0.98. The variation of median MAEs was smaller
 418 than 0.08t/ha. The median R s of emulator for spring wheat, however, tended to decline
 419 under 810ppm perturbation substantially and the median MAEs tended to increase
 420 simultaneously. Similarly, for nitrogen perturbation, the range of median R s was less
 421 than 0.15, and the range of median MAEs was smaller than 0.1t/ha, except for emulators
 422 of spring wheat and rice. The declined R and increased MAE were caused by the
 423 reduction of valid sample size from the GGCM output yield under CO₂ and nitrogen
 424 perturbations (Figure S7 & Figure S8).



425
 426 **Figure 8** Correlation coefficient (R) of multiple emulators ensemble under varied TW perturbations. The
 427 line denotes the median of R over current cropland, and the shaded area denotes the range of median R
 428 over current cropland across emulators.



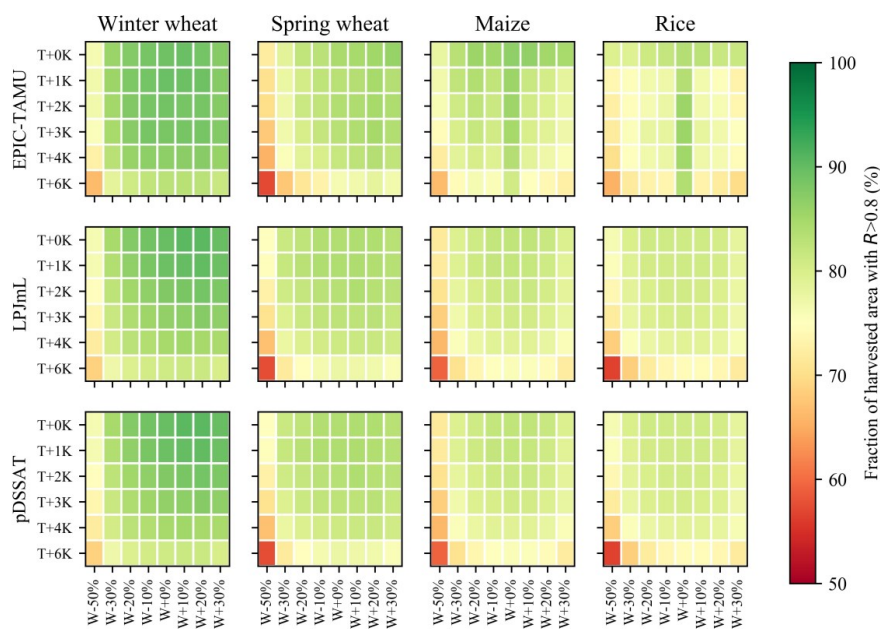
429
 430 **Figure 9** Mean absolute error (MAE) of multiple emulators ensemble under varied CTWN
 431 perturbations. The line denotes the median of R over current cropland, and the shaded area denotes
 432 the range of median R over current cropland across emulators.

433 3.3.4 Performance of multiple emulators at grid scale under dual perturbations

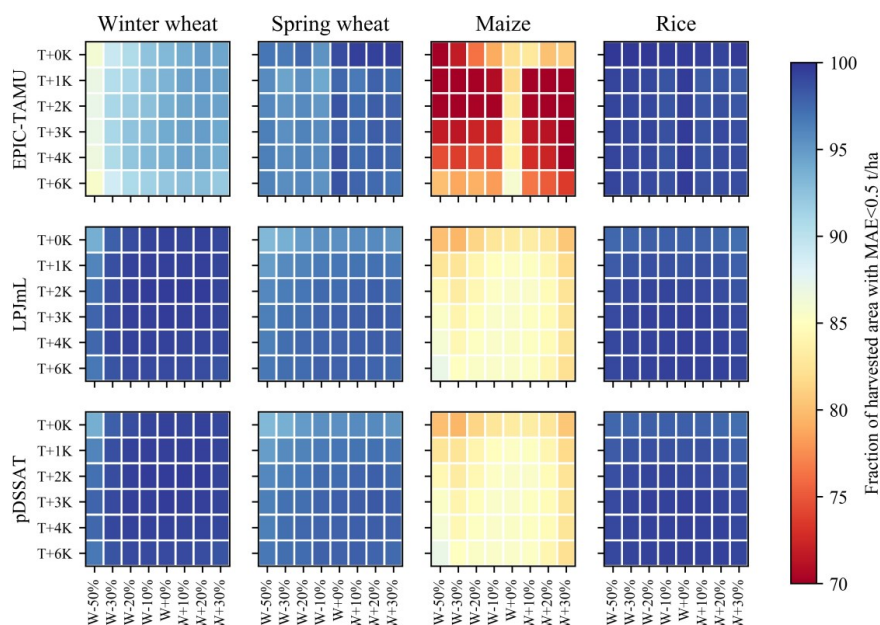
434 The performance of emulators was influenced by changes in simultaneous perturbations
 435 in two different CTWN dimensions (dual perturbations). The emulators performed well
 436 over most of current cropland but at extreme increases in T and reductions in W (**Figure**
 437 **10**), the emulators could represent the GGCM-simulated year-to-year variation only on
 438 substantially smaller shares of the current cropland. The fraction of current areas with
 439 R greater than 0.8 was the highest in the baseline but decreases under warmer and drier
 440 conditions. The fraction reduced to less than 60% under compound T+6K and W-50%
 441 perturbation, which illustrated the poor capacity of emulator under compound hot-dry
 442 conditions. However, the fraction of harvested areas with MAE smaller than 0.5 t/ha



443 did not vary much across T+W perturbations (**Figure 11**). The performance of emulators
 444 under dual perturbations for wheat were better than those for maize and rice. The
 445 fraction of maize and rice harvested area with R greater than 0.8 was relatively smaller
 446 than that of wheat. The maize harvested area with MAE smaller than 0.5 t/ha was
 447 smaller than other crops. Among the three GGCMs with full range of CTWN
 448 perturbations, the fraction of harvested area with high accuracy for LPJmL-emulator
 449 and pDSSAT-emulator was more than EPIC-TAMU-emulator.



450
 451 **Figure 10** Fraction of harvested areas with high correlation coefficient ($R > 0.8$) under varied T+W
 452 perturbations. Example of EPIC-TAMU-A0, LPJmL-A0 and pDSSAT-A0 emulator because only these
 453 three GGCMs contain full range of CTWN perturbations for all four crops.



454

455 **Figure 11** Fraction of harvested areas with low mean absolute error (MAE<0.5 t/ha)
456 under varied T+W perturbations. Example of EPIC-TAMU-A0, LPJmL-A0 and pDSSAT-A0 emulator because these three
457 GCMs contain full range of CTWN perturbations for all four crops.

458 4. Discussion

459 4.1 Emulator trained to capture year-to-year variation in crop yield

460 Our emulator was designed to reproduce the year-to-year variation of crop yield.
461 Therefore, the annual yield was the target variable in emulator fitting. To capture the
462 year-to-year crop yield variation well, the climatic predictors were divided into growing
463 season average, daily variation and climatic extremes to capture the possible drivers of
464 yield variation. The predictors engineering referred to the existing knowledges
465 compiled into crop models that year-to-year variation of crop yield is associated with
466 growing season temperature and precipitation (Ray et al., 2015), extreme heat (Iizumi
467 and Ramankutty, 2016) and drought (Heinicke et al., 2022). The temperature and
468 precipitation have been confirmed to be the dominant drivers to crop yield variability



469 (Schauberger et al., 2016). Moreover, the interaction between soil type and climate was
470 considered in our emulator design. Although CO₂ concentration and soil type were not
471 regarded as important contributors to yield variability, their interaction with climate
472 could also influence the yield variability (Kadam et al., 2014). The role of soil type has
473 been uncovered by previous emulator fitted by multivariate regression that the average
474 effect of temperature and precipitation differed greatly depending on soil type (Blanc,
475 2017). Compared with the emulator designed to reproduce the climatological mean
476 yield, our emulator is more suitable to project the changes in yield variability (Liu et
477 al., 2021b).

478

479 We developed the emulators with one statistical relationship for each crop between
480 GGCM simulated yield and predictors for all grids over global lands. Each grid cell
481 represents a sample in the soil-climate-fertilizer continuum, and the training data have
482 no lateral relationships. However, the response of simulated crop yield to climate
483 change was spatially heterogeneous, which mainly depends on the cultivars. Therefore,
484 one statistical relationship between yield and climatic predictors was hard to be fully
485 appropriate for each grid. In response, we used the length of growing season, a
486 representative predictor of cultivar characteristics, to adjust the global statistical
487 relationship to each grid. Therefore, predictors contained both temporal varied and
488 constant variables. The temporal varied predictors were climatic variables which
489 mainly played the role in reproduce the annual yield variation, and the temporal
490 constant predictors were non-climatic variables, like growing season length, delineated
491 the spatial distinction of crop yield response to climate. Compared with region-specific
492 emulator development, combining the temporal varied and constant predictors was
493 more concise and could profit from a broader range of data in the training set.

494 **4.2 Potential application of the well performed emulators in related fields**

495 The good performance over most grid cells indicated the potential capacity of emulators
496 in spatiotemporal downscaling, projecting annual yield in the future and multi-model



497 ensemble simulation.

498

499 The emulator could be used to conduct spatiotemporal yield downscaling because the
500 good performance of individual emulator in reproducing the annual crop yield variation
501 in the baseline. As the emulator in this study was developed with a regression-based
502 machine learning technique by using all the grid-year data points, the emulation is not
503 limited to the spatial resolution of the training data. The emulator can be applied to any
504 point with information on the predictors and can produce yield projections is as finely
505 resolved as the forcing input. From the aspect of time series of yield, the raw GGCM
506 data includes empty values (“NaN”) in some year-grid cell data points, which may be
507 caused by the lack of regional data for calibration. The vacancy of yield time series in
508 some grids could be imputed by the emulator (Folberth et al., 2019), similar to studies
509 which generated spatiotemporal continuous gridded crop yield data (Chen et al., 2022;
510 Iizumi et al., 2014).

511

512 The emulator was able to project the annual yield in the future climate scenarios, which
513 depends on the individual emulator performed well in reproducing annual yield under
514 CTWN cubes. In contrast to many previous emulators developed with historical crop
515 model simulations (Xu et al., 2021), our emulator could reproduce the CO₂ fertilization
516 effect which is an important forcing in future. The recently developed emulator based
517 on GGCM phase2 simulation under CTWN cubes could only project the
518 climatological-mean yield because the target variable in emulation was the
519 climatological-mean yield (Franke et al., 2020a). In contrast, our emulator can project
520 the annual yield variation and is not constrained by the maximum warming considered
521 in the GGCM phase2 data set (T+6K), but by the maximum temperature within the
522 training data set (warmest grid cell +6K), so that the applicability is broader (Müller et
523 al., 2021).

524

525 It is more efficient to conduct multi-model ensemble simulation with emulators than



526 GGCMs, as the emulators show good skill in reproducing GGCMs' results and the
527 emulators drastically reduce the computational time and memory requirement and
528 expertise to operate process-based crop models. First, the input of multiple emulators
529 was consistent and compatible but the inputs of raw GGCM were divergent and
530 incompatible because the structure of input data and file format of each GGCM was
531 designed independently. Second, the time-scale of emulator input was monthly or
532 growing seasonal, which was less complex than daily inputs of GGCMs. Apart from
533 the ensemble simulation, the multiple emulators could also be used to explore and
534 disentangle the uncertainty across models.

535 **4.3 Uncertainties**

536 The weaknesses of machine learning algorithm and raw GGCM have brought some
537 uncertainties into the emulators. The uncertainties induced by the machine learning
538 algorithm was as follows:

539

540 (1) When the climate factors went beyond the range of training data, the weakness of
541 machine learning in out-of-sample prediction could bring great uncertainty. The
542 emulator inputs should be capped by the range of training data. The limit of our
543 emulator was the warmest grid under +6K perturbation. As there is polar amplification,
544 the strongest warming mostly happens in cooler regions. Thus, the projected
545 temperature exceeding training range would not be widespread over global croplands.

546

547 (2) The random selection of testing samples in machine learning algorithm failed to
548 warrant independence from training samples when dependence structure exist in the
549 data (Meyer and Pebesma, 2021; Ploton et al., 2020). In our cross-validation, the
550 adjusted R^2 s were likely to be overestimated when using the 10-fold cross validation
551 approach with randomly selected trained and validated samples due to the spatial
552 autocorrelated simulated yield. By using the leave-one-out validation approach, the
553 overestimation of adjusted R^2 s has been reduced after excluding the spatial



554 autocorrelation. Yet, the emulators derived from the 10-fold cross validation and leave-
555 one-out validation approach are not directly comparable in terms of goodness-of-fit
556 statistics due to completely different parameters trained. We then carefully compared
557 the relative feature importance. As shown in Figure S9-S12, relative importance of
558 predictors was consistent across the two validation strategies. That said, the emulator
559 trained and validated by 10-fold cross-validation with randomly selected samples can
560 reproduce the climate-yield relationship similar to that derived from the leave-one-out
561 validation approach, in spite of over-estimation of the goodness-of-fit statistics. In
562 model application, we would suggest use the emulators derived from the 10-fold cross
563 validation due to its random sampling to avoid any potential biased estimation. But
564 users still should be cautious when describing the accuracy of the machine learning
565 based emulators. Still, model goodness-of-fits were reasonably good for
566 emulating. Considering the spatial autocorrelation when fitting a machine learning
567 model could provide a more objective understanding of model accuracy.

568

569 (3) Although the emulators could reproduce the GGCM annual yield with high accuracy
570 in most cases, there were cases that the machine learning algorithm did not show good
571 reproduction skill. As the emulated function intended to smooth the response of
572 simulated crop yield to climate, samples at the margins of training data tend to show
573 lower emulator skill. The extreme conditions, i.e. +6K, -50% water, 810ppm, 10kgN/ha,
574 show reduced R and increased MAE. Using the emulators to estimate annual crop yield
575 under extreme perturbation conditions should be conducted with caution and the additional
576 uncertainty induced by the emulators should be considered in the interpretation of
577 results.

578

579 (4) Last but not the least, as the emulators are intended as lightweight tools that could
580 replicate the raw GGCMs, their capability in simulating crop yields is limited to the
581 capability of the original GGCMs. This raises the issue that emulators are unlikely to
582 show good performance in simulating crop yield responses to climate extremes, exactly



583 like the raw GGCMs, which have shown poor performance in capturing the yield
584 impact of heatwave and drought (Heinicke et al., 2022), and the lack of negative effect
585 of excessive wetness (Li et al., 2019a). Resolving such a problem requires the
586 improvement of raw GGCMs' capability in simulating yield response to climate
587 extremes, or statistical promotion of the GGCMs' outputs under extreme weather events.

588 **5. Conclusion**

589 In this study, we developed the machine-learning based statistical crop yield emulators
590 to reproduce the year-to-year variation of crop yield to perturbations in CO₂
591 concentration, temperature, water and nitrogen-application rate from the GGCM phase
592 2 archives. To examine the potential value of these emulators, we evaluated the
593 performance of emulators at global and gridded scale under baseline, under single and
594 dual perturbations.

595

596 The results indicated that the performance of emulators was good enough to reproduce
597 the year-to-year variation of global average crop yield in the baseline ($R > 0.98$), and
598 the difference of accuracy between individual GGCM emulators were not large.
599 Similarly, under single and dual perturbations, the capacity of emulators in reproducing
600 the year-to-year variation of global mean crop yield was not substantially changed. At
601 gridded level, the performance of emulators over most of the current croplands in the
602 baseline was still good in the sense that R was greater than 0.8 and MAE was smaller
603 than 0.5 t/ha. The performance of individual emulators was consistently good under
604 single CTWN perturbations, without substantial changes in R and MAE. Similarly, the
605 multiple emulators also performed well in reproducing the annual yield under single
606 CTWN perturbations, and the most grid cells across the current cropland showed
607 greater R and smaller MAE under simultaneous perturbations of T and W. The overall
608 good capacity of emulators in reproducing the year-to-year variation of GGCM
609 simulated crop yield indicated the role of emulators in spatiotemporal downscaling,



610 crop yield projection and multi-model ensemble simulation. The emulators were able
611 to boost the ability to assess crop yield failure risk under future climate change and help
612 to better understand food stability and climate risk adaptation.
613



614 **Code availability**

615 The python function for crop model emulators are available at
616 <https://doi.org/10.5281/zenodo.7796686>

617 **Author contributions**

618 WL and TY designed the research. WL, TY and CM prepared the manuscript. All
619 authors contributed to editing the manuscript.

620 **Competing interests**

621 Some authors are members of the editorial board of GMD. The peer-review process
622 was guided by an independent editor, and the authors have also no other competing
623 interests to declare.

624 **Acknowledgment**

625 This study was supported by State Key Laboratory of Earth Surface Processes and
626 Resource Ecology of China (2022-ZD-06), the National Natural Science Foundation of
627 China (42171075).
628



629 References

- 630 Blanc, E. and Sultan, B.: Emulating maize yields from global gridded crop models using statistical
631 estimates, *Agric. For. Meteorol.*, 214–215, 134–147, doi:10.1016/j.agrformet.2015.08.256, 2015.
- 632 Blanc, É.: Statistical emulators of maize, rice, soybean and wheat yields from global gridded crop
633 models, *Agric. For. Meteorol.*, 236, 145–161, doi:10.1016/j.agrformet.2016.12.022, 2017.
- 634 Blanc, É.: Statistical emulators of irrigated crop yields and irrigation water requirements, *Agric. For.*
635 *Meteorol.*, 284(January), 107828, doi:10.1016/j.agrformet.2019.107828, 2020.
- 636 Campbell, B. M., Vermeulen, S. J., Girvetz, E., Loboguerrero, A. M. and Ramirez-Villegas, J.:
637 Reducing risks to food security from climate change, *Glob. Food Sec.*, 11, 34–43,
638 doi:10.1016/j.gfs.2016.06.002, 2016.
- 639 Chen, S., Liu, W., Feng, P., Ye, T., Ma, Y. and Zhang, Z.: Improving Spatial Disaggregation of Crop
640 Yield by Incorporating Machine Learning with Multisource Data: A Case Study of Chinese Maize
641 Yield, *Remote Sens.*, 14(10), doi:10.3390/rs14102340, 2022.
- 642 Chen, T. and Guestrin, C.: XGBoost: A Scalable Tree Boosting System, in *Proceedings of the 22Nd*
643 *ACM SIGKDD International Conference on Knowledge Discovery and Data Mining*, pp. 785–
644 794, ACM, New York, NY, USA., 2016.
- 645 Elliott, J., Müller, C., Deryng, D., Chrystanthopoulos, J., Boote, K. J., Büchner, M., Foster, I.,
646 Glotter, M., Heinke, J., Iizumi, T., Izaurralde, R. C., Mueller, N. D., Ray, D. K., Rosenzweig, C.,
647 Ruane, A. C. and Sheffield, J.: The Global Gridded Crop Model Intercomparison: data and
648 modeling protocols for Phase 1 (v1.0), *Geosci. Model Dev.*, 8(2), 261–277, doi:10.5194/gmd-8-
649 261-2015, 2015.
- 650 Folberth, C., Baklanov, A., Balkovič, J., Skalský, R., Khabarov, N. and Obersteiner, M.: Spatio-
651 temporal downscaling of gridded crop model yield estimates based on machine learning, *Agric.*
652 *For. Meteorol.*, 264(May 2018), 1–15, doi:10.1016/j.agrformet.2018.09.021, 2019.
- 653 Franke, J. A., Müller, C., Elliott, J., Ruane, A. C., Jägermeyr, J., Balkovic, J., Ciais, P., Dury, M.,
654 Falloon, P. D., Folberth, C., François, L., Hank, T., Hoffmann, M., Izaurralde, R. C., Jacquemin,
655 I., Jones, C., Khabarov, N., Koch, M., Li, M., Liu, W., Olin, S., Phillips, M., Pugh, T. A. M.,
656 Reddy, A., Wang, X., Williams, K., Zabel, F. and Moyer, E. J.: The GGCM Phase 2 emulator:
657 Global gridded crop model response to changes in CO₂, temperature, water, and nitrogen
658 (protocol version 1.0), *Geosci. Model Dev.*, 13(5), 2315–2336, doi:10.5194/gmd-13-2315-2020,
659 2020a.
- 660 Franke, J. A., Müller, C., Elliott, J., Ruane, A. C., Jägermeyr, J., Balkovic, J., Ciais, P., Dury, M.,
661 Falloon, P. D., Folberth, C., François, L., Hank, T., Hoffmann, M., Izaurralde, R. C., Jacquemin,
662 I., Jones, C., Khabarov, N., Koch, M., Li, M., Liu, W., Olin, S., Phillips, M., Pugh, T. A. M.,
663 Reddy, A., Wang, X., Williams, K., Zabel, F. and Moyer, E. J.: The GGCM Phase 2 experiment:
664 Global gridded crop model simulations under uniform changes in CO₂, temperature, water, and
665 nitrogen levels (protocol version 1.0), *Geosci. Model Dev.*, 13(5), 2315–2336, doi:10.5194/gmd-
666 13-2315-2020, 2020b.
- 667 Frieler, K., Schauburger, B., Arneth, A., Balkovič, J., Elliott, J., Folberth, C., Deryng, D., Müller, C.,
668 Olin, S., Pugh, T. A. M., Schaphoff, S., Schewe, J., Schmid, E., Warszawski, L. and Levermann,
669 A.: Understanding the weather signal in national crop-yield variability Earth ’ s Future, *Earth ’ s*
670 *Futur.*, 5, 605–616, doi:10.1002/ef2.217, 2017.



- 671 Fronzek, S., Pirttioja, N., Carter, T. R., Bindi, M., Hoffmann, H., Palosuo, T., Ruiz-Ramos, M., Tao, F.,
672 Trnka, M., Acutis, M., Asseng, S., Baranowski, P., Basso, B., Bodin, P., Buis, S., Cammarano, D.,
673 Deligios, P., Destain, M. F., Dumont, B., Ewert, F., Ferrise, R., François, L., Gaiser, T., Hlavinka,
674 P., Jacquemin, I., Kersebaum, K. C., Kollas, C., Krzyszczak, J., Lorite, I. J., Minet, J., Minguez,
675 M. I., Montesino, M., Moriondo, M., Müller, C., Nendel, C., Öztürk, I., Perego, A., Rodríguez, A.,
676 Ruane, A. C., Ruget, F., Sanna, M., Semenov, M. A., Slawinski, C., Stratonovitch, P., Supit, I.,
677 Waha, K., Wang, E., Wu, L., Zhao, Z. and Rötter, R. P.: Classifying multi-model wheat yield
678 impact response surfaces showing sensitivity to temperature and precipitation change, *Agric.*
679 *Syst.*, 159(June 2017), 209–224, doi:10.1016/j.agsy.2017.08.004, 2018.
- 680 Hasegawa, T., Sakurai, G., Fujimori, S., Takahashi, K., Hijioka, Y. and Masui, T.: Extreme climate
681 events increase risk of global food insecurity and adaptation needs, *Nat. Food*, 2(8), 587–595,
682 doi:10.1038/s43016-021-00335-4, 2021.
- 683 Heinicke, S., Frieler, K., Jägermeyr, J. and Mengel, M.: Global gridded crop models underestimate
684 yield responses to droughts and heatwaves, *Environ. Res. Lett.*, 0–68 [online] Available from:
685 <https://iopscience.iop.org/article/10.1088/1748-9326/ac592e>, 2022.
- 686 Iizumi, T. and Ramankutty, N.: Changes in yield variability of major crops for 1981–2010 explained by
687 climate change, *Environ. Res. Lett.*, 11(3), 34003, doi:10.1088/1748-9326/11/3/034003, 2016.
- 688 Iizumi, T., Yokozawa, M., Sakurai, G., Travasso, M. I., Romanenkov, V., Oettli, P. and Newby, T.:
689 Historical changes in global yields : major cereal and legume crops from 1982 to 2006, , 346–357,
690 doi:10.1111/geb.12120, 2014.
- 691 Jägermeyr, J., Robock, A., Elliott, J., Muller, C., Xia, L., Khabarov, N., Folberth, C., Schmid, E., Liu,
692 W., Zabel, F., Rabin, S. S., Puma, M. J., Heslin, A., Franke, J., Foster, I., Asseng, S., Bardeen, C.
693 G., Toon, O. B. and Rosenzweig, C.: A regional nuclear conflict would compromise global food
694 security, *Proc. Natl. Acad. Sci. U. S. A.*, 117(13), 7071–7081, doi:10.1073/pnas.1919049117,
695 2020.
- 696 Jägermeyr, J., Müller, C., Ruane, A., Elliott, J., Balkovic, J., Castillo, O., Faye, B., Foster, I., Folberth,
697 C., Franke, J., Fuchs, K., Guarin, J., Heinke, J., Hoogenboom, G., Iizumi, T., Jain, A. ., Kelly, D.,
698 Khabarov, N., Lange, S., Lin, T., Liu, W., Mialyk, O., Minol, S. and Rosenzweig, C.: Climate
699 change signal in global agriculture emerges earlier in new generation of climate and crop models,
700 *Nat. Food* (in Revis.), 2021.
- 701 Janssens, C., Havlik, P., Krisztin, T., Baker, J., Frank, S., Hasegawa, T., Leclère, D., Ohrel, S.,
702 Ragnauth, S., Schmid, E., Valin, H., Van Lipzig, N. and Maertens, M.: Global hunger and climate
703 change adaptation through international trade, *Nat. Clim. Chang.*, 10(9), 829–835,
704 doi:10.1038/s41558-020-0847-4, 2020.
- 705 Jones, J. W., Antle, J. M., Basso, B., Boote, K. J., Conant, R. T., Foster, I., Godfray, H. C. J., Herrero,
706 M., Howitt, R. E., Janssen, S., Keating, B. A., Munoz-Carpena, R., Porter, C. H., Rosenzweig, C.
707 and Wheeler, T. R.: Brief history of agricultural systems modeling, *Agric. Syst.*, 155, 240–254,
708 doi:10.1016/j.agsy.2016.05.014, 2017.
- 709 Kadam, N. N., Xiao, G., Melgar, R. J., Bahuguna, R. N., Quinones, C., Tamilselvan, A., Prasad, P. V.
710 V and Jagadish, K. S. V: Chapter Three - Agronomic and Physiological Responses to High
711 Temperature, Drought, and Elevated CO₂ Interactions in Cereals, vol. 127, edited by D. B. T.-A.
712 in A. Sparks, pp. 111–156, Academic Press., 2014.
- 713 Kinnunen, P., Guillaume, J. H. A., Taka, M., D’Odorico, P., Siebert, S., Puma, M. J., Jalava, M. and
714 Kumm, M.: Local food crop production can fulfil demand for less than one-third of the



- 715 population, *Nat. Food*, 1(4), 229–237, doi:10.1038/s43016-020-0060-7, 2020.
- 716 Li, Y., Guan, K., Schnitkey, G. D., DeLucia, E. and Peng, B.: Excessive rainfall leads to maize yield
717 loss of a comparable magnitude to extreme drought in the United States, *Glob. Chang. Biol.*,
718 25(7), 2325–2337, doi:10.1111/gcb.14628, 2019a.
- 719 Li, Y., Guan, K., Yu, A., Peng, B., Zhao, L., Li, B. and Peng, J.: Toward building a transparent
720 statistical model for improving crop yield prediction: Modeling rainfed corn in the U.S, *F. Crop.*
721 *Res.*, 234(January), 55–65, doi:10.1016/j.fcr.2019.02.005, 2019b.
- 722 Liu, W., Ye, T. and Shi, P.: Decreasing wheat yield stability on the North China Plain: Relative
723 contributions from climate change in mean and variability, *Int. J. Climatol.*, 41(S1), E2820–
724 E2833, doi:10.1002/joc.6882, 2021a.
- 725 Liu, W., Ye, T., Jägermeyr, J., Müller, C., Chen, S., Liu, X. and Shi, P.: Future climate change
726 significantly alters interannual wheat yield variability over half of harvested areas, *Environ. Res.*
727 *Let.*, 16(9), 094045, doi:10.1088/1748-9326/ac1fbb, 2021b.
- 728 Liu, W., Li, Z., Li, Y., Ye, T., Chen, S. and Liu, Y.: Heterogeneous impacts of excessive wetness on
729 maize yields in China: Evidence from statistical yields and process-based crop models, *Agric. For.*
730 *Meteorol.*, 327(August), 109205, doi:10.1016/j.agrformet.2022.109205, 2022.
- 731 Lobell, D. B., Sibley, A. and Ivan Ortiz-Monasterio, J.: Extreme heat effects on wheat senescence in
732 India, *Nat. Clim. Chang.*, 2(3), 186–189, doi:10.1038/nclimate1356, 2012.
- 733 Makowski, D., Asseng, S., Ewert, F., Bassu, S., Durand, J. L., Li, T., Martre, P., Adam, M., Aggarwal,
734 P. K., Angulo, C., Baron, C., Basso, B., Bertuzzi, P., Biernath, C., Boogaard, H., Boote, K. J.,
735 Bouman, B., Bregaglio, S., Brisson, N., Buis, S., Cammarano, D., Challinor, A. J., Confalonieri,
736 R., Conijn, J. G., Corbeels, M., Deryng, D., De Sanctis, G., Doltra, J., Fumoto, T., Gaydon, D.,
737 Gayler, S., Goldberg, R., Grant, R. F., Grassini, P., Hatfield, J. L., Hasegawa, T., Heng, L., Hoek,
738 S., Hooker, J., Hunt, L. A., Ingwersen, J., Izaurrealde, R. C., Jongschaap, R. E. E., Jones, J. W.,
739 Kemanian, R. A., Kersebaum, K. C., Kim, S. H., Lizaso, J., Marcaida, M., Müller, C., Nakagawa,
740 H., Naresh Kumar, S., Nendel, C., O’Leary, G. J., Olesen, J. E., Oriol, P., Osborne, T. M.,
741 Palosuo, T., Pravia, M. V., Priesack, E., Ripoche, D., Rosenzweig, C., Ruane, A. C., Ruget, F.,
742 Sau, F., Semenov, M. A., Shcherbak, I., Singh, B., Singh, U., Soo, H. K., Steduto, P., Stöckle, C.,
743 Stratonovitch, P., Streck, T., Supit, I., Tang, L., Tao, F., Teixeira, E. I., Thorburn, P., Timlin, D.,
744 Travasso, M., Rötter, R. P., Waha, K., Wallach, D., White, J. W., Wilkens, P., Williams, J. R.,
745 Wolf, J., Yin, X., Yoshida, H., Zhang, Z. and Zhu, Y.: A statistical analysis of three ensembles of
746 crop model responses to temperature and CO₂ concentration, *Agric. For. Meteorol.*, 214–215,
747 483–493, doi:10.1016/j.agrformet.2015.09.013, 2015.
- 748 Meyer, H. and Pebesma, E.: Predicting into unknown space? Estimating the area of applicability of
749 spatial prediction models, *Methods Ecol. Evol.*, 12(9), 1620–1633, doi:10.1111/2041-
750 210X.13650, 2021.
- 751 Mistry, M. N., Sue Wing, I. and De Cian, E.: Simulated vs. empirical weather responsiveness of crop
752 yields: US evidence and implications for the agricultural impacts of climate change, *Environ. Res.*
753 *Let.*, 12(7), doi:10.1088/1748-9326/aa788c, 2017.
- 754 Müller, C., Franke, J., Jägermeyr, J., Ruane, A. C., Elliott, J., Moyer, E., Heinke, J., Falloon, P.,
755 Folberth, C., Francois, L., Hank, T., Izaurrealde, R. C., Jacquemin, I., Liu, W., Olin, S., Pugh, T.,
756 Williams, K. E. and Zabel, F.: Exploring uncertainties in global crop yield projections in a large
757 ensemble of crop models and CMIP5 and CMIP6 climate scenarios, *Environ. Res. Let.*,
758 doi:10.1088/1748-9326/abd8fc, 2021.



- 759 Nachtergaele, F., Velthuizen, H. Van, Verelst, L., Batjes, N., Dijkshoorn, K., Engelen, V. Van, Fischer,
760 G., Jones, A., Montanarella, L., Petri, M., Prieler, S., Teixeira, E., Wiberg, D. and Shi, X.:
761 Harmonized World Soil Database (version 1), *Soil Sci.*, p.38, doi:3123, 2009.
- 762 Ostberg, S., Schewe, J., Childers, K. and Frieler, K.: Changes in crop yields and their variability at
763 different levels of global warming, *Earth Syst. Dyn.*, 9(2), 479–496, doi:10.5194/esd-9-479-2018,
764 2018.
- 765 Pirttioja, N., Carter, T. R., Fronzek, S., Bindi, M., Hoffmann, H., Palosuo, T., Ruiz-Ramos, M., Tao, F.,
766 Trnka, M., Acutis, M., Asseng, S., Baranowski, P., Basso, B., Bodin, P., Buis, S., Cammarano, D.,
767 Deligios, P., Destain, M. F., Dumont, B., Ewert, F., Ferrise, R., François, L., Gaiser, T., Hlavinka,
768 P., Jacquemin, I., Kersebaum, K. C., Kollas, C., Krzyszczak, J., Lorite, I. J., Minet, J., Minguez,
769 M. I., Montesino, M., Moriondo, M., Müller, C., Nendel, C., Öztürk, I., Perego, A., Rodríguez, A.,
770 Ruane, A. C., Ruget, F., Sanna, M., Semenov, M. A., Slawinski, C., Stratonovitch, P., Supit, I.,
771 Waha, K., Wang, E., Wu, L., Zhao, Z. and Rötter, R. P.: Temperature and precipitation effects on
772 wheat yield across a European transect: A crop model ensemble analysis using impact response
773 surfaces, *Clim. Res.*, 65, 87–105, doi:10.3354/cr01322, 2015.
- 774 Ploton, P., Mortier, F., Réjou-Méchain, M., Barbier, N., Picard, N., Rossi, V., Dormann, C., Cornu, G.,
775 Viennois, G., Bayol, N., Lyapustin, A., Gourlet-Fleury, S. and Pélissier, R.: Spatial validation
776 reveals poor predictive performance of large-scale ecological mapping models, *Nat. Commun.*,
777 11(1), 1–11, doi:10.1038/s41467-020-18321-y, 2020.
- 778 Portmann, F. T., Siebert, S. and Döll, P.: MIRCA2000—Global monthly irrigated and rainfed crop
779 areas around the year 2000: A new high-resolution data set for agricultural and hydrological
780 modeling, *Global Biogeochem. Cycles*, 24(1), doi:10.1029/2008GB003435, 2010.
- 781 Raimondo, M., Nazzaro, C., Marotta, G. and Caracciolo, F.: Land degradation and climate change:
782 Global impact on wheat yields, *L. Degrad. Dev.*, 32(1), 387–398, doi:10.1002/ldr.3699, 2021.
- 783 Ray, D. K., Gerber, J. S., Macdonald, G. K. and West, P. C.: Climate variation explains a third of
784 global crop yield variability, *Nat. Commun.*, 6, 1–9, doi:10.1038/ncomms6989, 2015.
- 785 Ruane, A. C., Goldberg, R. and Chryssanthacopoulos, J.: Climate forcing datasets for agricultural
786 modeling: Merged products for gap-filling and historical climate series estimation, *Agric. For.
787 Meteorol.*, 200, 233–248, doi:10.1016/j.agrformet.2014.09.016, 2015.
- 788 Sacks, W. J., Deryng, D., Foley, J. A. and Ramankutty, N.: Crop planting dates: an analysis of global
789 patterns, *Glob. Ecol. Biogeogr.*, 19(5), 607–620, doi:10.1111/j.1466-8238.2010.00551.x, 2010.
- 790 Schauburger, B., Rolinski, S. and Müller, C.: A network-based approach for semi-quantitative
791 knowledge mining and its application to yield variability, *Environ. Res. Lett.*, 11(12),
792 doi:10.1088/1748-9326/11/12/123001, 2016.
- 793 Shahhosseini, M., Martinez-Feria, R. A., Hu, G. and Archontoulis, S. V.: Maize yield and nitrate loss
794 prediction with machine learning algorithms, *Environ. Res. Lett.*, 14(12), 124026,
795 doi:10.1088/1748-9326/ab5268, 2019.
- 796 Sternberg, T.: Regional drought has a global impact, *Nature*, 472(7342), 169–169,
797 doi:10.1038/472169d, 2011.
- 798 Tartarini, S., Vesely, F., Movedi, E., Radegonda, L., Pietrasanta, A., Recchi, G. and Confalonieri, R.:
799 Biophysical models and meta-modelling to reduce the basis risk in index-based insurance: A case
800 study on winter cereals in Italy, *Agric. For. Meteorol.*, 300, 108320,
801 doi:https://doi.org/10.1016/j.agrformet.2021.108320, 2021.
- 802 Troy, T. J., Kipgen, C. and Pal, I.: The impact of climate extremes and irrigation on US crop yields,



803 Environ. Res. Lett., 10(5), 1–10, doi:10.1088/1748-9326/10/5/054013, 2015.
804 Xu, H., Zhang, X., Ye, Z., Jiang, L., Qiu, X., Tian, Y., Zhu, Y. and Cao, W.: Machine learning
805 approaches can reduce environmental data requirements for regional yield potential simulation,
806 Eur. J. Agron., 129(August 2020), doi:10.1016/j.eja.2021.126335, 2021.
807 Zhu, X. and Troy, T. J.: Agriculturally Relevant Climate Extremes and Their Trends in the World's
808 Major Growing Regions, Earth's Futur., 6(4), 656–672, doi:10.1002/2017EF000687, 2018.
809